Magnetic ordering in trigonal chain compounds[☆]

V. Eyert [a,*], U. Schwingenschlögl [a], C. Hackenberger [a],
T. Kopp [a], R. Frésard [b], U. Eckern [a]

[a] *Institut für Physik, Universität Augsburg, 86135 Augsburg, Germany*
[b] *Laboratoire Crismat, UMR CNRS-ENSICAEN (ISMRA) 6508, Caen, France*

Abstract

We present electronic structure calculations for the one-dimensional magnetic chain compounds Ca_3CoRhO_6 and Ca_3FeRhO_6. The calculations are based on density functional theory and the local density approximation. We use the augmented spherical wave (ASW) method. The observed alternation of low- and high-spin states along the Co−Rh and Fe−Rh chains is related to differences in the oxygen coordination of the transition metal sites. Due to strong hybridization the O 2p states are polarized, giving rise to extended localized magnetic moments centered at the high-spin sites. Strong metal−metal overlap along the chains leads to a substantial contribution of the low-spin Rh $4d_{3z^2-r^2}$ orbitals to the exchange coupling of the extended moments. Interestingly, this mechanism holds for both compounds, even though the coupling is ferromagnetic for cobalt and antiferromagnetic for the iron compound. However, our results allow to understand the different types of coupling from the filling dependence of the electronic properties.

1. Introduction

The perovskite family of oxides shows a great compositional variety. Recently, a new structural class of hexagonal perovskites has started to attract increasing attention due to their

---

[☆] This paper was originally submitted as part of the International Conference on Perovskites at EMPA, 2005, Properties and Potential Applications special Issue.
 * Corresponding author. Tel.: +49 821 598 3246; fax: +49 821 598 3262.
   E-mail address: eyert@physik.uni-augsburg.de (V. Eyert).

extraordinary magnetic properties. These materials are based on the general formula A'_3ABO_6 (A' = alkaline earth; A and B = transition metal) and crystallize in the trigonal K_4CdCl_6 structure [1] with space group $R\bar{3}c$ (D^6_{3d}, No. 167). In these compounds, transition metal—oxygen polyhedra form well separated chains running parallel to the trigonal axis; see Refs. [2,3] for a representation of the crystal structure. Space between the chains is filled with the A' cations. Each chain consists of alternating, face-sharing AO_6 trigonal prisms and BO_6 octahedra. Typically, the ratio of interchain to small intrachain metal—metal distance is of the order of two, the fact explaining the importance of metal—metal bonding and the pronounced one-dimensionality. The chains themselves are arranged on a triangular lattice. As a consequence, in addition to showing the abovementioned unique properties these compounds allow to study geometric frustration effects such as partial disorder and spin-glass like behaviour.

A prominent member of this class is $Ca_3Co_2O_6$, which has two inequivalent cobalt sites, one in octahedral environment (labelled Co1) and the other (Co2) centered in the trigonal prisms [2,3]. Neutron diffraction measurements revealed low- and high-spin moments of 0.08 μ_B and 3.00 μ_B, respectively, at these sites. Together with susceptibility measurements they point towards a ferromagnetic coupling along the chains, and an antiferromagnetic one in the buckling $a-b$ plane. Susceptibility [4,5], specific heat [5], and μ-SR [6] measurements clearly demonstrate the onset of three-dimensional ordering at $T_{C_1} = 24$ K, while a second transition was found at $T_{C_2} = 12$ K [4,7]. Magnetization measurements showed a plateau at ≈ 1.31 μ_B per f.u. for low field and a steep increase by a factor of three at about 3.5 T, which was interpreted as a ferri- to ferromagnetic transition [3,4]. In addition, the magnetization versus field curves display a rich structure below 12 K [8]. In particular, the magnetization at saturation exceeds the (spin only) expected value of 4 μ_B/f.u., indicating that the angular momentum is not fully quenched. Electronic structure calculations revealed (i) low- and high-spin moments, respectively, at the octahedral and trigonal prismatic cobalt sites in good agreement with the experimental data, (ii) a rather large oxygen moment due to polarization by the high-spin cobalt sites, which together give rise to the formation of extended but still well localized CoO_6 moments, and (iii) strong contributions to the ferromagnetic intrachain coupling from the 3d states of the low-spin octahedral cobalt atoms [9]. Recently, mapping these results onto a Heisenberg model we were able to underline the importance of the interplay of different crystal field splittings, d—p hybridizations, and metal—metal overlap for the ferromagnetic intrachain order [10,11].

Nevertheless, the origin of the ferromagnetic intrachain coupling is still a matter of intense debate. In order to resolve the issue we have turned to the related compounds Ca_3CoRhO_6 and Ca_3FeRhO_6, which have the same crystal structure as $Ca_3Co_2O_6$ as well as very similar electronic properties [12]. However, while Ca_3CoRhO_6 likewise shows ferromagnetic intrachain order, the coupling is antiferromagnetic in the iron compound. Hence, by studying these systems we will contribute to a deeper understanding of the underlying exchange mechanisms.

To be specific, according to susceptibility and neutron diffraction measurements Ca_3CoRhO_6 undergoes two transitions at $T_{C_1} = 90$ K and $T_{C_2} = 30$ K, which are attributed to the ferromagnetic intrachain and the antiferromagnetic interchain coupling, respectively [13—16]. However, the specific heat did not exhibit any strong anomaly at these temperatures [17]. Thus, elucidating the nature of the transitions requires more investigations. Again, the interaction across the chains is antiferromagnetic driving the system into a partially disordered antiferromagnetic (PDA) state at intermediate temperatures. However, application of small magnetic fields results in a ferrimagnetic phase [18]. Neutron diffraction data suggest both the cobalt and rhodium ions to be trivalent [14,19]. Spin states are $S = 2$ at the trigonal prismatic cobalt sites and $S = 0$ at the octahedral rhodium sites. The magnetic moment amounts to 3.7 μ_B per cobalt ion and is oriented parallel to the c-axis.

The magnetic ordering of Ca_3FeRhO_6 turns out to be less complex than in the cobaltate. Susceptibility data reveal a single transition into a three-dimensional antiferromagnetic phase at 12 K [13,16] with the easy axis oriented parallel to the chains as well as divalent iron in a $S = 2$ high-spin state and tetravalent rhodium in a $S = 1/2$ low-spin state. In contrast, Mössbauer experiments were interpreted in favour of trivalent iron and $S = 5/2$ [20]. For the saturation magnetization a value of 3.74 μ_B per f.u. has been given [20].

2. Methodology

The density functional calculations were performed using the scalar-relativistic augmented spherical wave (ASW) method [21,22]. In order to represent the correct shape of the crystal potential in the large voids of the open crystal structure, additional augmentation spheres were inserted. Optimal augmentation sphere positions as well as radii of all spheres were automatically generated by the sphere geometry optimization (SGO) algorithm [23]. Self-consistency was achieved by an efficient algorithm for convergence acceleration [24]. Brillouin zone sampling was done using an increased number of **k**-points ranging from 28 to 770 points within the irreducible wedge.

3. Results and discussion

Using the powder data of Niitaka et al. [13], we performed, in a first step, a set of calculations, where spin-degeneracy was enforced [12]. The results are shown in Fig. 1, which includes the partial densities of states of both Ca_3CoRhO_6 and Ca_3FeRhO_6. While we observe O 2p dominated bands between -6.8 and -2.4 eV, three groups of bands of mainly metal d-character are found at higher energies. Due to d–p hybridization substantial p/d contributions appear above/below -2 eV, reaching up to 40% in the upper valence and conduction bands.

At the rhodium sites, the octahedral crystal field leads to nearly perfect splitting of the 4d states into occupied t_{2g} and empty e_g states. In contrast, the trigonal crystal field at the
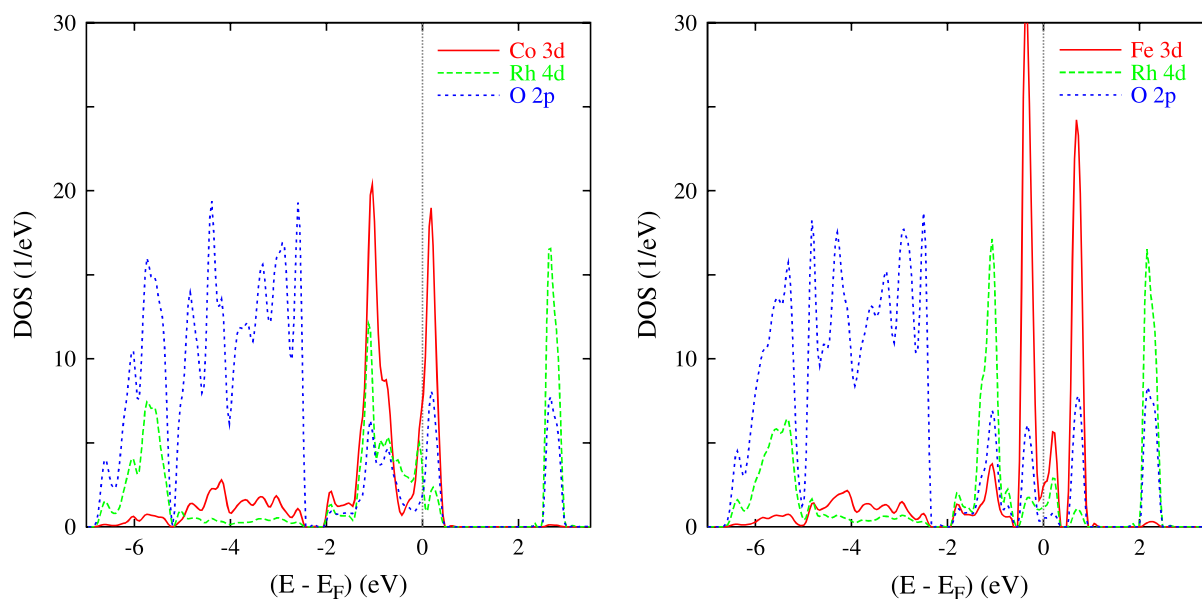

Fig. 1. Partial densities of states of Ca_3CoRhO_6 and Ca_3FeRhO_6.

cobalt/iron sites results in a splitting into non-degenerate $d_{3z^2-r^2}$ as well as doubly degenerate d_{xy,x^2-y^2} and $d_{xz,yz}$ states. While, due to strong σ-type d—p bonding, the Rh 4d e_g states form the high-energy peak above 2.0 eV, the peak below traces back to Co/Fe $d_{xz,yz}$ states. As a consequence, spin-polarization of the latter bands is highly favourable explaining the observed high-spin/low-spin scenario.

Spin-polarized calculations performed in a second step lead to the observed ferromagnetic and antiferromagnetic behaviour found for Ca_3CoRhO_6 and Ca_3FeRhO_6, respectively. As a result, we obtained well localized magnetic moments of 0.48 μ_B (Rh), 2.59 μ_B (Co), 0.14 μ_B (O), and 0.00 μ_B (Ca) for the cobaltate as well as 0.00 μ_B (Rh), 3.72 μ_B (Fe), 0.14 μ_B (O), and 0.01 μ_B (Ca) for the ferrate. These values reflect the experimental result of low- and high-spin states at the octahedral and trigonal prismatic sites, respectively. The total moment per unit cell (i.e. per two formula units) amounts to 7.94 μ_B for Ca_3CoRhO_6 and ±4.59 μ_B per sublattice in Ca_3FeRhO_6. Worth mentioning are the rather high magnetic moments at the oxygen sites arising from the strong d—p hybridization, which sum up to about 1 μ_B per trigonal prism. Adding to the 3d moment they lead to the formation of extended localized moments already observed in $Ca_3Co_2O_6$ [9] and confirms the formal Fe $S = 5/2$ and Rh $S = 0$ spin configurations.

According to a more detailed analysis the increased iron moment as compared to that of cobalt arises from the energetical upshift of the bands due to the reduced electron count and can be attributed to the d_{xy,x^2-y^2} orbitals. However, since these orbitals point perpendicular to the chain axis their contribution affects mainly the size of the local moment and to a much lesser degree the intrachain coupling.

In order to understand this puzzling result we turn back to the spin-degenerate calculations and investigate the near-E_F bands, which are displayed in Figs. 2 and 3. The length of the bars appended to the bands is a measure of the contributions of the respective orbitals. Note that these orbitals refer to the global coordinate system with the z-axis along the chain direction. Obviously, all bands display strong dispersion parallel to the chain axis (i.e. the line Γ—A), reflecting the one-dimensionality of the compounds, while weak dispersions perpendicular to this line indicate small interchain coupling. According to Figs. 2 and 3, the most strongly dispersing bands are of almost pure $d_{3z^2-r^2}$ character with similar contributions from both transition metal
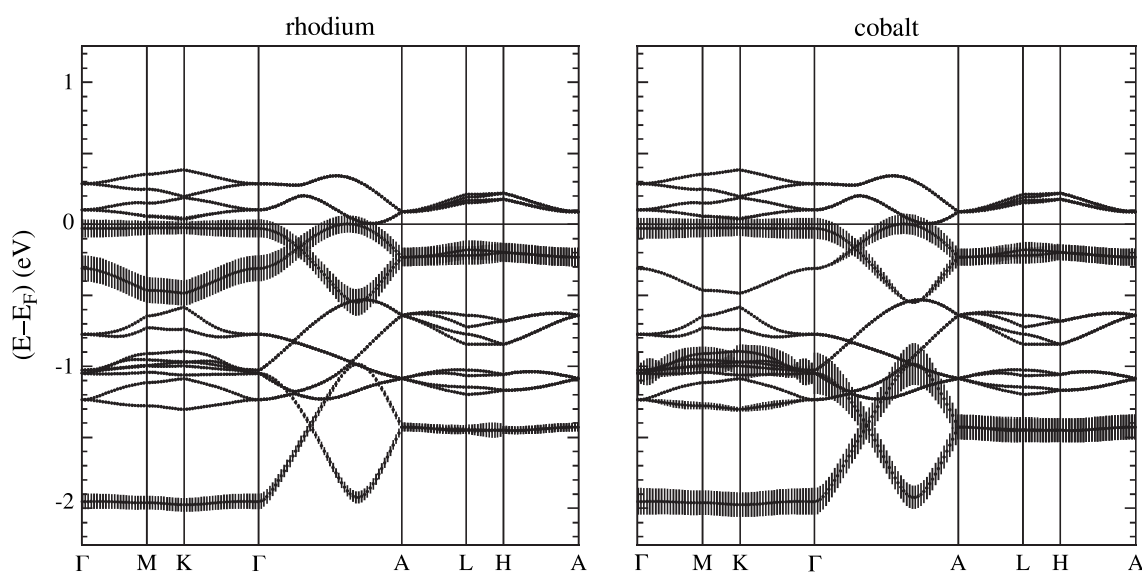

Fig. 2. Weighted electronic bands of spin-degenerate Ca_3CoRhO_6. Contributions of the Rh $4d_{3z^2-r^2}$ (left) and Co $3d_{3z^2-r^2}$ (right) orbitals are indicated by bars.
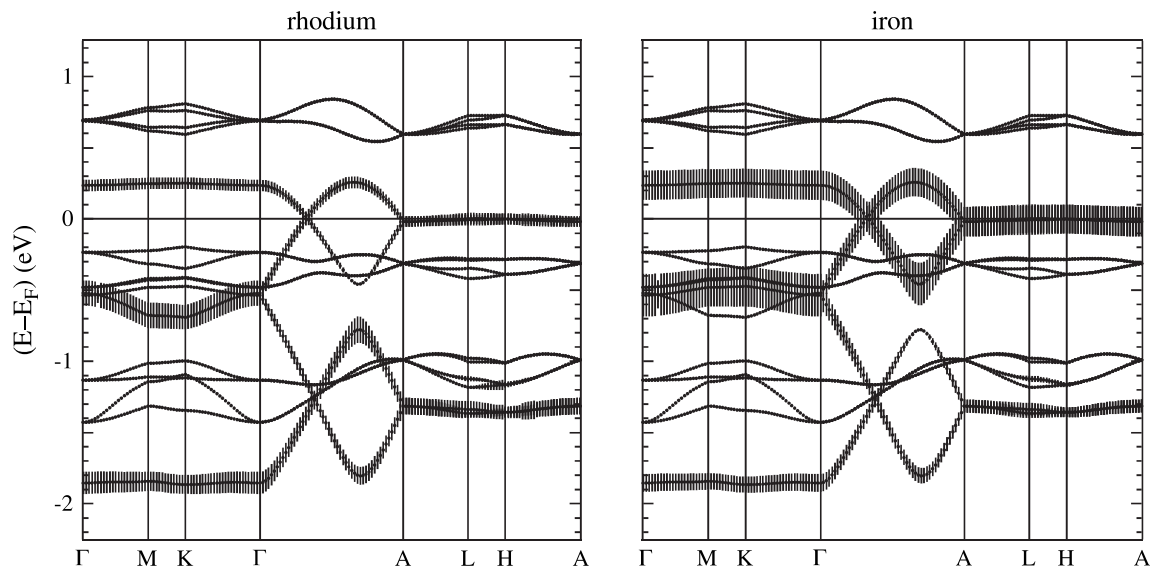
Fig. 3. Weighted electronic bands of spin-degenerate Ca_3FeRhO_6. Contributions of the Rh $4d_{3z^2-r^2}$ (left) and Fe $3d_{3z^2-r^2}$ (right) orbitals are indicated by bars.

sites, pointing to the strong metal—metal bonding within the chains. While the band dispersions are quite similar for both cobaltates and the ferrate, important differences arise from the reduced band filling in the latter, which drastically alters the Fermi surface. In general, due to the almost perfect one-dimensional dispersion, Fermi surfaces consist of flat sheets perpendicular to the c-axis, i.e. the line Γ—A. However, while in the cobaltates the z-position of Fermi surface is at the Γ-point, we observe perfect nesting in Ca_3FeRhO_6 with Fermi surface sheets at the A-point. As a consequence, the ferrate, but not the cobaltates, is susceptible to a Fermi surface instability against an antiferrodistortive mode or else the observed antiferromagnetic intrachain order.

4. Conclusion

As for the previously investigated $Ca_3Co_2O_6$, electronic structure calculations for Ca_3CoRhO_6 and Ca_3FeRhO_6 reveal strong effects of the local coordination on the electronic and magnetic properties. In particular, low- and high-spin moments are obtained at the octahedral Rh sites and at the trigonal prismatic Co/Fe sites, respectively. Strong d—p hybridization results in considerable oxygen polarization, giving rise to the formation of extended magnetic moments localized at the prisms. Metal—metal bonding via Rh $4d_{3z^2-r^2}$ orbitals lays ground for large contributions to the intrachain exchange coupling. Differences between the cobaltates and the ferrate due to the reduced electron count in the latter show up in the additional polarization of the Fe $3d_{xy,x^2-y^2}$ states. Furthermore, the corresponding band shifts have drastic effects for the Fermi surface, leading to almost perfect nesting and an A-point instability, which drive the observed antiferromagnetic intrachain order.

Acknowledgements

References

[1] Stitzer KE, Darriet J, zur Loye H-C. Curr Opin Solid State Mater Sci 2001;5:535.
[2] Fjellvåg H, Gulbrandsen E, Aasland S, Olsen A, Hauback BC. J Solid State Chem 1996;124:190.
[3] Aasland S, Fjellvåg H, Hauback BC. Solid State Commun 1997;101:187.
[4] Kageyama H, Yoshimura K, Kosuge K, Mitamura H, Goto T. J Phys Soc Jpn 1997;66:1607.
[5] Hardy V, Lambert S, Lees MR, Paul DMcK. Phys Rev B 2003;68:014424.
[6] Sugiyama J, Nozaki H, Brewer JH, Ansaldo EJ, Takami T, Ikuta H, et al. Phys Rev B 2005;72:064418.
[7] Maignan A, Michel C, Masset AC, Martin C, Raveau B. Eur Phys J B 2000;15:657.
[8] Hardy V, Lees MR, Petrenko OA, Paul DMcK, Flahaut D, Hébert S, et al. Phys Rev B 2004;70:064424.
[9] Eyert V, Laschinger C, Kopp T, Frésard R. Chem Phys Lett 2004;385:249.
[10] Laschinger C, Kopp T, Eyert V, Frésard R. J Magn Magn Mater 2004;272—276:974.
[11] Frésard R, Laschinger C, Kopp T, Eyert V. Phys Rev B 2004;69:140405(R).
[12] Schwingenschlögl U. Ph.D. thesis, Universität Augsburg, Berlin: Logos Verlag; 2004 [ISBN 3-8325-0530-X].
[13] Niitaka S, Kageyama H, Kato M, Yoshimura K, Kosuge K. J Solid State Chem 1999;146:137.
[14] Niitaka S, Yoshimura K, Kosuge K, Nishi M, Kakurai K. Phys Rev Lett 2001;87:177202.
[15] Niitaka S, Yoshimura K, Kosuge K, Mitsuda A, Mitamura H, Goto T. J Phys Chem Solids 2002;63:999.
[16] Davis MJ, Smith MD, zur Loye H-C. J Solid State Chem 2003;173:122.
[17] Hardy V, Lees MR, Maignan A, Hébert S, Flahaut D, Paul DMcK. J Phys Condens Matter 2003;15:5737.
[18] Niitaka S, Kageyama H, Yoshimura K, Kosuge K, Kawano S, Aso N, et al. J Phys Soc Jpn 2001;70:1222.
[19] Loewenhaupt M, Schäfer W, Niazi A, Sampathkumaran EV. Europhys Lett 2003;63:374.
[20] Niitaka S, Yoshimura K, Kosuge K, Mibu K, Mitamura H, Goto T. J Magn Magn Mater 2003;260:48.
[21] Williams AR, Kübler J, Gelatt Jr CD. Phys Rev B 1979;19:6094.
[22] Eyert V. Int J Quantum Chem 2000;77:1007.
[23] Eyert V, Höck K-H. Phys Rev B 1998;57:12727.
[24] Eyert V. J Comput Phys 1996;124:271.